that are close to the collision limit. The absence of any marked dependence of the rate coefficients on pressure signifies that the two association reactions are approaching the pressure-saturation regime. Schiff and Bohme[20] report a value of 2×10^{-9} cm^3 s^{-1} for the association of CH_3^+ to HCN at pressures of ~0.5 torr. Kemper et al.[21] from low-pressure ICR measurements have estimated a ternary rate coefficient $\sim 2 \times 10^{-25}$ cm^6 s^{-1} for association with HCN in He as the bath gas. The even more rapid association of CH_3^+ to CH_3CN occurs almost at the ion-dipole collision limit[22] ($k_{AADO} = 5.7 \times 10^{-9}$ cm^3 s^{-1}) and will presumably exhibit an even larger value for the ternary rate coefficient than the reaction of CH_3^+ with HCN.

Conclusions

Protonated CH_3CN and CH_3NC have different structures in the gas phase and maintain their integrity by a substantial isomerization barrier which prevents interconversion. The product ion of reaction 1 is a ~6/1 mixture of the two isomers of $C_2H_4N^+$, with CH_3CNH^+ being produced in the greater amount.

Acknowledgment. We wish to thank the New Zealand Universities Grants Committee for financial support.

Registry No. THP, 142-68-7; $THPH^+$, 27659-94-5; THF, 109-99-9; $THFH^+$, 27659-93-4; CH_3N, 75-05-8; CH_3NC, 593-75-9; $CH_3CN{\cdot}H^+$, 20813-12-1; $CH_3NC{\cdot}H^+$, 64709-60-0; CH_3^+, 14531-53-4; HCN, 74-90-8; HC(O)OMe, 107-31-3; NH_3, 7664-41-7; EtOEt, 60-29-7; NH_4^+, 14798-03-9; $EtOEtrH^+$, 17009-83-5; CH_3CHO, 75-07-0.

(20) Schiff, H. I.; Bohme, D. K. *Astrophys. J.* **1979**, *232*, 740.
(21) Kemper, P. R.; Bass, L. M.; Bowers, M. T. *J. Phys. Chem.* **1985**, *89*, 1105.
(22) Su, T.; Su, E. C. F.; Bowers, M. T. *J. Chem. Phys.* **1978**, *69*, 2243.
(23) Baghal-Vayjooee, M. H.; Collister, J. L.; Pritchard, H. O. *Can. J. Chem.* **1977**, *55*, 2634.

(24) **Note Added in Proof.** Recently a value of 834 kJ mol^{-1} for PA(CH_3NC) has been reported: Meot-ner, M.; Karpas, Z.; Deakyne, C. *J. Am. Chem. Soc.*, in press. This value agrees with the result reported here within the combined experimental uncertainties.

Diabatic Surface Methods for the Study of the Reactivity of Organic Molecules. 1. Cycloaddition of Two Ethylenes

Fernando Bernardi,*[1a] Massimo Olivucci,[1a] Michael A. Robb,*[1b] and Glauco Tonachini[1a,c]

Contribution from the Istituto Chimico G. Ciamician and Istituto di Chimica Organica, Università, 40100 Bologna, Italy, and Department of Chemistry, Queen Elizabeth College, London W8 7AH, England. *Received February 6, 1985*

Abstract: In this paper we discuss the quantitative diabatic surface analysis of the surface associated with the thermal cycloaddition of two ethylene molecules. We show that the main features of a saddle point, such as the index (i.e., the number of negative eigenvalues of the Hessian) and the origin, can be understood by analyzing the behavior of the reactant and product diabatic surfaces computed in a three-dimensional subspace involving two relevant geometrical variables at a time. We show also that the behavior of the constituent diabatic surfaces can be easily rationalized with the simple energy expressions of qualitative MO theory.

I. Introduction

One of the major development areas in quantum chemistry in recent years has involved the computation and characterization of the intermediates and transition structures for model organic reactions. The rapid growth of this research has been facilitated by the development of the MC-SCF method (for a recent review see ref 2) and gradient optimization techniques. In recent work we have been involved in the development of MC-SCF[3] gradient[4] programs and in the subsequent analysis of the reaction profile using diabatic surfaces.[5-8] In ref 6 we have shown that the transition structure geometry of the cyanate-isocyanate rearrangement, the 1,2-sigmatropic shift in propene, the S_N2 reaction of H^- and CH_4, and the addition of singlet methylene to ethylene correlate very accurately with the intersection of appropriate diabatic curves. In the case of the sigmatropic shift we were able to locate the transition structure a priori from preliminary diabatic surface calculations.

In the diabatic surface model[5,6] the adiabatic surface of the reaction is obtained from the interaction of two diabatic surfaces (one associated with reactants and one with products). The transition structure corresponds to the minimum of the surface of intersection of the two diabatic surfaces. This model stems from the very early work of Evans and Polanyi[9] and Evans and Warhurst.[10] The significant feature of the model proposed in ref 5 and 6 is the association of each diabatic surface with the bonding situation in reactants or products through the use of wave functions built from the molecular orbitals of the isolated fragments. Thus the diabatic surfaces are based upon a linear combination of fragment configurations (Heitler-London, no-bond, charge transfer, and locally excited).

In the present paper we discuss the diabatic surface analysis of the potential surface associated with the thermal cycloaddition of two ethylene molecules. The critical points (transition structures, intermediate minima, etc.) have been computed in a previous MC-SCF study.[11]

In our previous work on the diabatic surface model[5,6] we have followed a procedure similar to that used in the qualitative diabatic decomposition schemes[12-16] and considered only cross sections

(1) (a) Università di Bologna. (b) Queen Elizabeth College, London. (c) Permanent address: Istitutio di Chimica Organica, 10100 Torino, Italy.
(2) Olsen, J.; Yeager, D. L.; Jorgensen, P. *Adv. Chem. Phys.* **1983**, *55*, 1-4.
(3) Eade, H. A.; Robb, M. A. *Chem. Phys. Lett.* **1981**, *83*, 362-368.
(4) Schlegel, H. B.; Robb, M. A. *Chem. Phys. Lett.* **1982**, *93*, 43-46.
(5) Bernardi, F.; Robb, M. A. *Mol. Phys.* **1983**, *48*, 1345-1355.
(6) Bernardi, F.; Robb, M. A. *J. Am. Chem. Soc.* **1984**, *106*, 54-58.
(7) Bernardi, F.; Robb, M. A.; Schlegel, H. B.; Tonachini, G. *J. Am. Chem. Soc.* **1984**, *106*, 1198-1202.
(8) Bernardi, F.; Bottoni, A.; Robb, M. A. *Theor. Chim. Acta* **1984**, *64*, 259-263.
(9) Evans, M. G.; Polanyi, M. *Trans. Faraday Soc.* **1938**, *34*, 11-29.
(10) Evans, M. G.; Warhurst, E. *Trans. Faraday Soc.* **1938**, *34*, 614-624.
(11) Bernardi, F.; Bottoni, A.; Robb, M. A.; Schlegel, H. B.; Tonachini, G. *J. Am. Chem. Soc.* **1985**, *107*, 2260-2264.
(12) Simmons, H. E., Bunnett, J. F., Eds. "Orbital Symmetry Papers"; American Chemical Society: Washington, D.C., 1974.

0002-7863/86/1508-1408$01.50/0

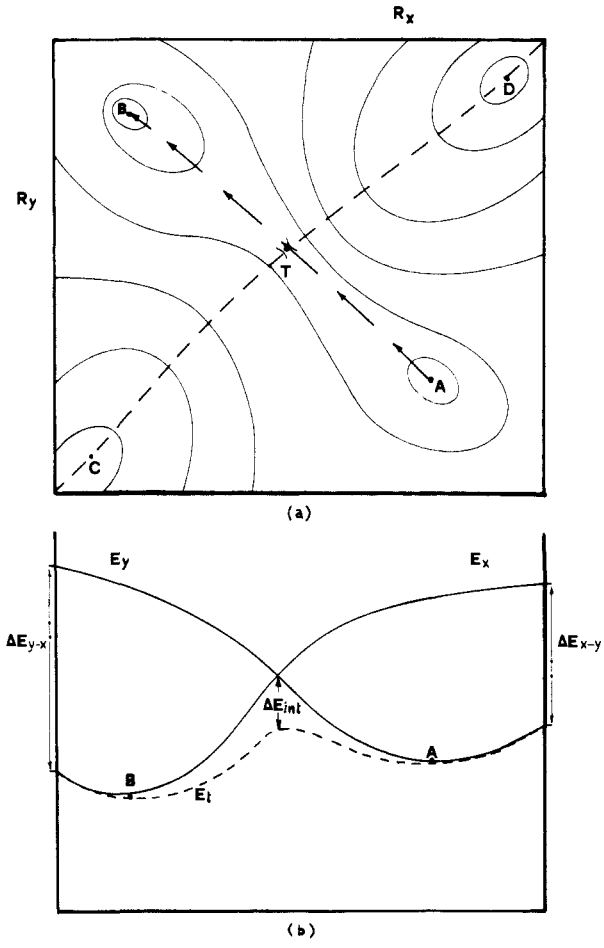

Figure 1. (a) Potential energy contour map for the reaction X ⇌ Y and (b) related adiabatic and diabatic curves.

through the diabatic surfaces along an assumed reaction coordinate. In such two-dimensional analysis, the crossing between two diabatic curves is usually associated with a transition state. However, a transition state is a maximum along the reaction coordinate and a minimum along the other coordinates. In other words it is a saddle point with index[17] equal to 1 (the index of a critical point is equal to the number of negative eigenvalues of the Hessian matrix). Therefore a transition state cannot be clearly identified in terms of a two-dimensional analysis, since at this level it is not possible to distinguish between a saddle point with index equal to 1 or larger than 1. In the present work we show that a clear understanding of the main features of a saddle point, such as index and origin, can be obtained from the analysis of the intersection of the diabatic surfaces in a subspace which involves two geometrical variables at a time, i.e., from the analysis of a series of three-dimensional diabatic surfaces.

Further, we are able to show that the qualitative behavior of the computed diabatic surfaces can be rationalized in terms of the familiar MO interaction diagrams of qualitative MO theory and the associated energy expressions.

II. The Diabatic Surface Model

Let us consider the reaction

$$X \rightleftharpoons Y \qquad (1)$$

and assume that the adiabatic surface can be described in terms of two variables R_x and R_y. We assume also that we can model the reaction surface with two diabatic surfaces $E_x(R_x,R_y)$ and $E_y(R_x,R_y)$. The surface $E_x(R_x,R_y)$ describes the bonding situation appropriate to the species X at all regions of the configuration space and similarly the surface $E_y(R_x,R_y)$ describes that appropriate to the species Y. Figure 1 illustrates a situation of this type. In Figure 1a we show a potential energy contour map. Points A and B are the minima associated with the reactants (X) and the products (Y), respectively. Point T is the transition state, and we assume that the line AB represents the "reaction coordinate". The dashed line C–D represents the "line of intersection" between the two diabatic surfaces. Clearly the transition state (point T) is at the maximum of the energy profile along the "reaction coordinate" and at the minimum along the "line of intersection". In Figure 1b we show a cross section of the surface shown in Figure 1a along the "reaction coordinate". The dashed curve represents the adiabatic curve (denoted with E_T) and the E_x and E_y curves the related diabatic components. The point of intersection corresponds to the transition state. We denote also with ΔE_{int} the stabilization energy associated with the interaction of the two diabatic components and with ΔE_{y-x} and ΔE_{x-y} the reactant and product excitation energies.

In our approach the decomposition in terms of diabatic surfaces is used to analyze the main features of a given reaction surface. In this model the rationalization of reactivity trends is based upon the following three quantities (see Figure 1): (i) the excitation energies ΔE_{y-x} and ΔE_{x-y}, (ii) the slope and shape of the diabatic surfaces, and (iii) the interaction energy ΔE_{int}.

The translation into rigorous quantum mechanical methods of the diabatic surface model based upon interacting fragment configurations built from the MO's of the isolated fragments has been discussed in our previous work[5,6] and will be only briefly summarized here. Let us assume that the wave function for the adiabatic surface can be represented by a CI expansion

$$\Psi = \sum_k C_k \Phi_k \qquad (2)$$

for all values of the reaction coordinates R_x and R_y. The Φ_k are configuration state functions built from the orbitals of some noninteracting fragments, which could be chosen by setting R_x to ∞, R_y to ∞ or both.

It is convenient to distinguish three types of orbitals: (i) core orbitals which are doubly occupied in all configurations, (ii) valence (or active) orbitals which have all possible occupancies in the Φ_k, and (iii) virtual orbitals which are unoccupied in all configurations. In general the valence orbitals will correspond to those orbitals involved in bond making and bond breaking. We can distinguish two types of configurations: configurations corresponding to antisymmetrized products of isolated fragment configurations (IFC) and charge-transfer configurations (CTC) corresponding to electron transfer between fragments. The IFC include Heitler–London-type configurations (HLC), which involve spin-paired open-shell fragments, and no-bond configurations (NBC), which refer to closed-shell configurations of the fragments.

In general we can identify a bonding situation and therefore describe the associated diabatic surface, with a combination of IFC, that correlates with given spectroscopic states of the fragments. In order to describe this "bonding situation" at a finite interfragment separation, we must add charge-transfer configurations subject to the constraint that we explicitly exclude any IFC that describes a different "bonding situation". Thus a diabatic surface is constructed from a wave function containing a subset of IFC and CTC that describes a "specific bonding situation" and explicitly excludes others.

In order to satisfy the chemist's need to understand and develop a simple qualitative model, the main features of the diabatic surfaces can be rationalized in terms of very simple MO arguments. In fact, as we shall presently show, each specific bonding situation can be associated with an MO interaction diagram with specific orbital occupancies, whose energy effect can be discussed in terms of simple MO expressions. Therefore in our approach we compute exactly the diabatic surfaces with the procedure

(13) Epiotis, N. D. "Theory of Organic Reactions"; Springer-Verlag: Heidelberg, 1978.
(14) Epiotis, N. D. *Lect. Notes Chem.* **1982**, 29.
(15) Woodward, R. B.; Hoffmann, R. "The Conservation of Orbital Symmetry"; Academic Press: New York, 1970.
(16) (a) Shaik, S. S. *J. Am. Chem. Soc.* **1981**, *103*, 3692–3701. (b) Shaik, S. S. *J. Am. Chem. Soc.* **1982**, *104*, 2708–2719. (c) Shaik, S. S. *Nouv. J. Chim.* **1982**, *6*, 159–161.
(17) Mezey, P. G. Optimization and Analysis of Energy Hypersurfaces, In "Computational Theoretical Organic Chemistry"; Reidel Publishing Co.: New York, 1981.

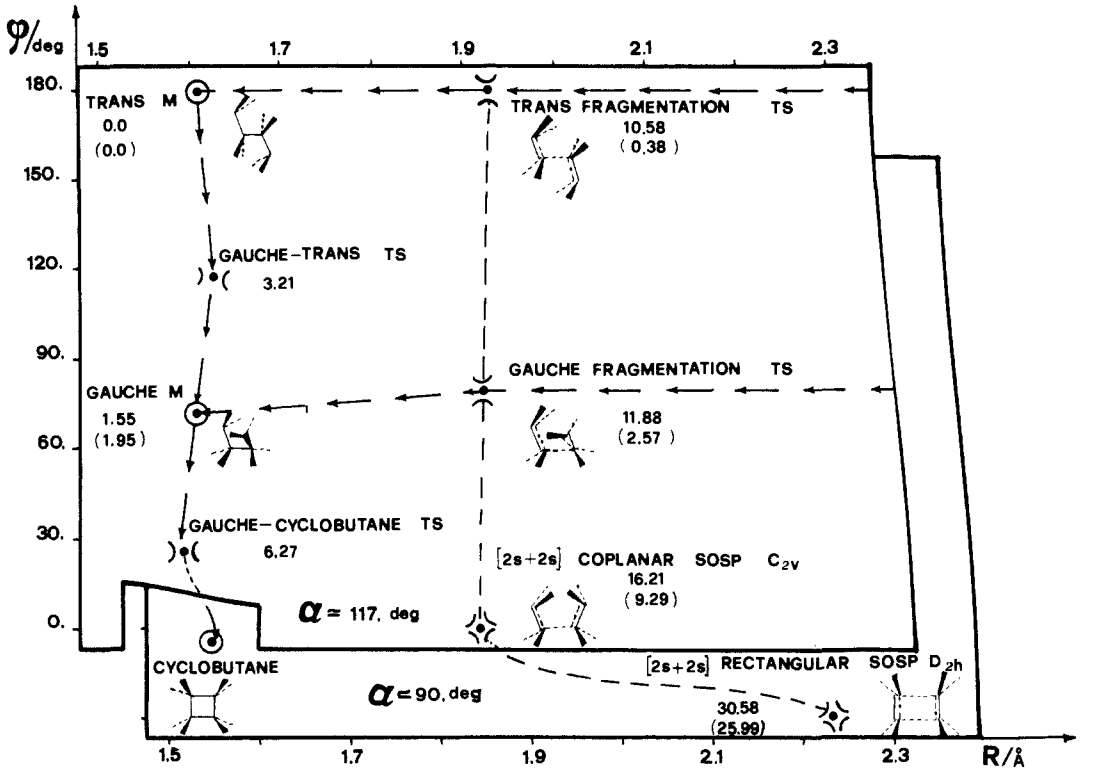

Figure 2. Critical points of the surface associated with the cycloaddition of two ethylenes (M denotes a minimum, TS a transition state, and SOSP a second-order saddle point). The energies are given relative to the energy of the trans tetramethylene diradical minimum and are computed at the STO-3G (4-31G) level.

Scheme I

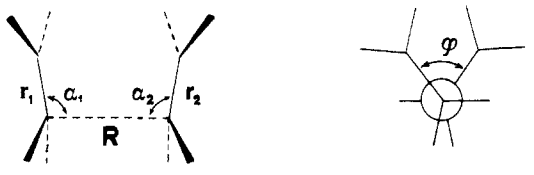

previously described[5,6] and then we rationalize their behavior in terms of two MO interaction diagrams, one specific for the "bonding situation" of the reactants and the other for the "bonding situation" of the products.

III. Analysis of the Ethylene–Ethylene Surface

Recently we have performed an ab initio MC–SCF study of the transition structure region of the thermal cycloaddition of two ethylene molecules, where the various critical points have been fully optimized with MC–SCF gradients and characterized by computing the corresponding hessian matrices.[11] In this section we apply the procedure previously described to rationalize the main features of the computed ethylene–ethylene surface. We shall focus our attention upon the region of the surface corresponding to the supra–supra, the gauche, and the trans approaches. According to the MC–SCF results, this is the region of the surface which is chemically important. There is also the region involving the supra–antara approach; however, this region is energetically isolated and thus chemically less relevant. Consequently, we shall discuss the features of the supra–antara surface separately in a subsequent paper.

The results obtained in the MC–SCF study are illustrated in Figure 2 in terms of an R,φ map (for the notation of the internal coordinates see Scheme I). In this map it is possible to include, with some approximations, all the critical points of the chemically important region of the surface, except that for the $|2_s + 2_s|$ rectangular coplanar approach, which belongs to a different cross section. For the latter, in fact, the value of α is 90°, while the α values of all the other critical points vary between 110 and 117°. The most important results obtained in the MC–SCF study can be summarized as follows: (i) Both the gauche and trans approaches involve a transition state and a diradicaloid minimum. Thus there are two local minima for the tetramethylene diradical corresponding to a gauche and a trans geometry. In the tetramethylene diradical region, in addition to the two fragmentation transition states, we have found two other transition states, one connecting the trans and gauche minima and the other along the path connecting the gauche minimum to cyclobutane. (ii) The supra–supra approach involves two saddle points with index equal to 2, one for a rectangular coplanar approach where D_{2h} symmetry is maintained and the other for a coplanar approach where C_{2v} symmetry is maintained.

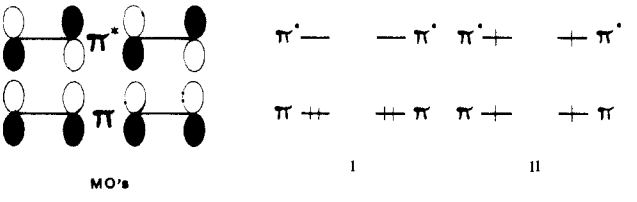

Figure 3. Valence orbitals for the addition of two ethylenes and IFC associated with reactants (I) and products (II).

All computations presented here have been performed at the STO-3G level,[18] since, as previously shown,[11] the main features of the various critical points are well reproduced at this computational level. Integral calculations have been performed with the GAUSSIAN 80 series of programs,[19] and the CI and MC–SCF codes are described in ref 20.

For our diabatic surface analysis we take as fragments the two ethylene molecules and take as valence orbitals the π and π^* MO's of the two ethylenes. The reactant IFC (configuration I in Figure

(18) Hehre, W. J.; Stewart, R. F.; Pople, J. A. *J. Chem. Phys.* **1969**, *51*, 2657–2664.
(19) Binkley, J. S.; Whiteside, R. A.; Krishnan, R.; Seeger, R.; De Frees, D. J.; Schlegel, H. B.; Topiol, S.; Kahn, L. R.; Pople, J. A. *QCPE* **1981**, *13*, 406.
(20) (a) Hegarty, D.; Robb, M. A. *Mol. Phys.* **1979**, *38*, 1795–1812. (b) Robb, M. A.; Eade, R. H. A. *Nato Adv. Study Inst. Ser., Ser. C* **1981**, *67*, 21–54.

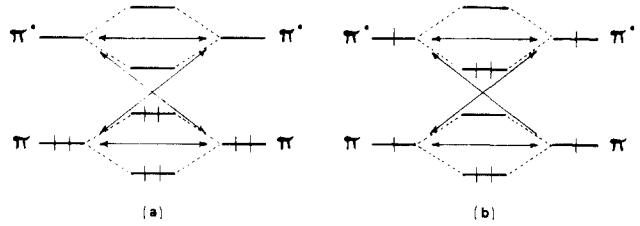

Figure 4. Interaction diagrams involving the π MO's of two ethylene molecules for the reactants (a) and products (b).

3) involves the singlet states of the two fragments, while the product IFC (configuration II in Figure 3) correponds to two ethylenes in a triplet state with the overall spin coupled to a singlet. Thus the two diabatic surfaces are associated with these two IFC plus the related one-electron CTC. In the case of configuration II, where there are four unpaired electrons, there is the possibility of coupling two pairs in two singlets and then coupling the result to an overall singlet or coupling first to two triplets then to a singlet. The packet II contains both possibilities but is dominated by the triplet–triplet coupling and correlates at infinite separation with the triplet states of the two ethylenes.

The two diabatic surfaces thus defined can be associated with the two interaction diagrams shown in Figure 4, which refer to the interaction of the π MO's of two singlet ethylenes in one case and of two triplet ethylenes coupled to a singlet in the other case. In other words our computational procedure provides a quantitative measure of the energy variation associated with these two interaction diagrams.[21]

The advantage of associating a given diabatic surface with an interaction diagram is that the energy effect associated with the interaction diagram, and consequently the energy behavior of the diabatic surface, can be rationalized qualitatively in terms of simple MO expressions which describe the energy effects of the various types of orbital interactions involved. In the present case (see Figure 4), in the reactant interaction diagram there are only two types of orbital interactions, i.e., a destabilizing four-electron interaction and a stabilizing two-electron interaction, whose energy effects are described by eq 3 and 4, respectively. In the product interaction diagram there are only stabilizing interactions between singly occupied orbitals. The stabilization energy associated with the interaction of two singly occupied orbitals is described by eq 5 when they are degenerate.

$$\Delta E_{ij}^{4} = 4\frac{(S_{ij}^{2}\epsilon_0 - S_{ij}H_{ij})}{1 - S_{ij}^{2}} \simeq K_1 S_{ij}^{2} \qquad \left(K_1 = \frac{4(\epsilon_0 - K)}{1 - S_{ij}^{2}} > 0\right) \quad (3)$$

$$\Delta E_{ij}^{2} = 2\frac{(H_{ij} - S_{ij}\epsilon_i)^2}{\epsilon_i - \epsilon_j} \simeq K_2\frac{S_{ij}^{2}}{\epsilon_i - \epsilon_j} \qquad (K_2 = 2(K - \epsilon_i)^2 > 0) \quad (4)$$

$$\Delta E_{ij}^{2'} = 2\frac{H_{ij} - \epsilon_i S_{ij}}{1 + S_{ij}} \simeq K_3 S_{ij} \qquad \left(K_3 = \frac{2(K - \epsilon_i)}{1 + S_{ij}} < 0\right) \quad (5)$$

These expressions are the usual perturbation formulas.[22-26]

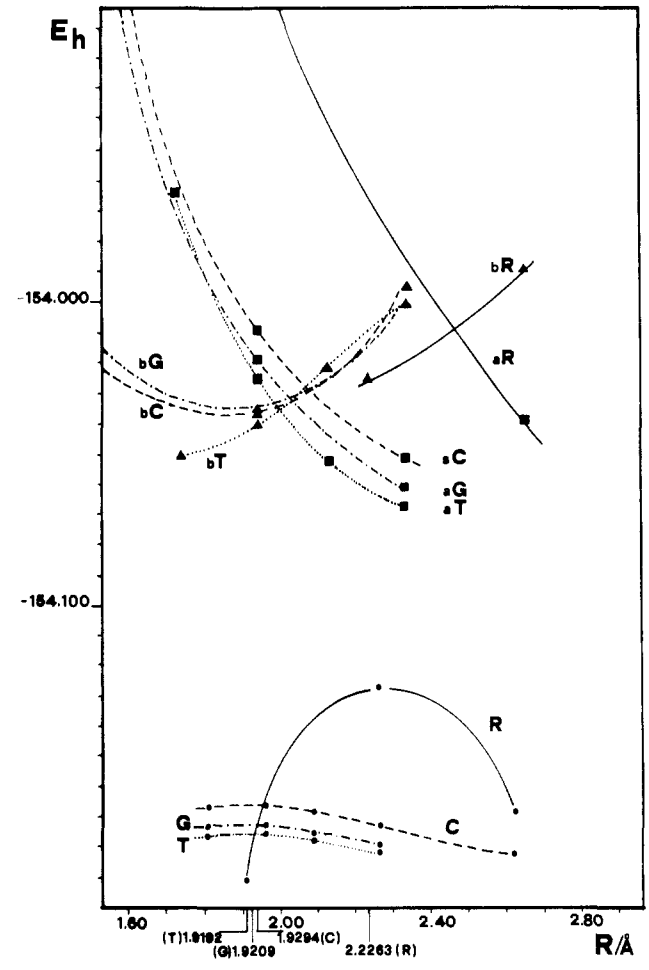

Figure 5. Adiabatic and reactant (a) and product (b) diabatic curves along R for the rectangular (R) and coplanar (C) supra-supra, gauche (G) and trans (T) approaches. The numerical values denote the STO-3G optimized R values of the various critical points.

Here ϵ_i and ϵ_j denote the energies of the two interacting MO's, S_{ij} their overlap integral, H_{ij} their interaction matrix element, and ϵ_0 the mean of the orbital energies. Since in a comparative analysis of a given surface the overlap is the main variable quantity, we have expressed the various formulas in terms of S_{ij}. To this purpose we have made use of the assumption that the interaction matrix element H_{ij} is proportional to the overlap integral S_{ij}, i.e., $H_{ij} = KS_{ij}$[27] $(K < 0)$.

We begin our discussion by examining some cross sections of the diabatic surfaces for the various types of approach. The various types of adiabatic and diabatic curves along the interfragment distance R are shown in Figure 5. In these computations we have used for the ethylene fragments the geometries optimized at the STO-3G level for the corresponding critical points. In each type of approach, with the decrease of R, the reactant diabatic curve increases rapidly and the product diabatic curve decreases. In each case there is an intersection of the two diabatic curves which occurs very near to the optimized R value of the corresponding critical point.

The behavior of these diabatic curves with R can be simply rationalized. In each case, in the reactant interaction diagram the dominant orbital interaction is the destabilizing four-electron interaction π–π. Since the related overlap and destabilization

(21) In some particular cases the two diabatic surfaces can be computed also within a conventional MO-CI. For instance, in the case of a D_{2h} supra–supra approach, the configuration associated with the reactants is, with reference to Figure 4, $(\pi + \pi)^2\,(\pi - \pi_2)^2$, while that associated with the products is $(\pi + \pi)^2\,(\pi^* + \pi^*)^2$ and their energy behavior can be simply computed in terms of a 2 × 2 CI involving the HOMO and LUMO of the two interacting ethylenes. However, in the majority of cases the reactant and product diabatic surfaces cannot be characterized at the MO level.

(22) Hoffmann, R. *Acc. Chem. Res.* **1971**, *4*, 1–9.

(23) Salem, L. *J. Am. Chem. Soc.* **1968**, *90*, 543–552.

(24) Dewar, M. J. S. "The Molecular Orbital Theory of Organic Chemistry"; McGraw-Hill: New York, 1969.

(25) Epiotis, N. D.; Cherry, W. R.; Shaik, S.; Yates, R. L.; Bernardi, F. *Top. Curr. Chem.* **1977**, 70.

(26) Hudson, R. F. *Angew. Chem. Int., Ed. Engl.* **1973**, *12*, 36–56.

(27) McGlynn, S. P.; Vanquickenborne, L. G.; Kinoshita, M.; Carrol, D. G. "Introduction to Applied Quantum Chemistry"; Holt, Rinchart and Winston: New York, 1972.

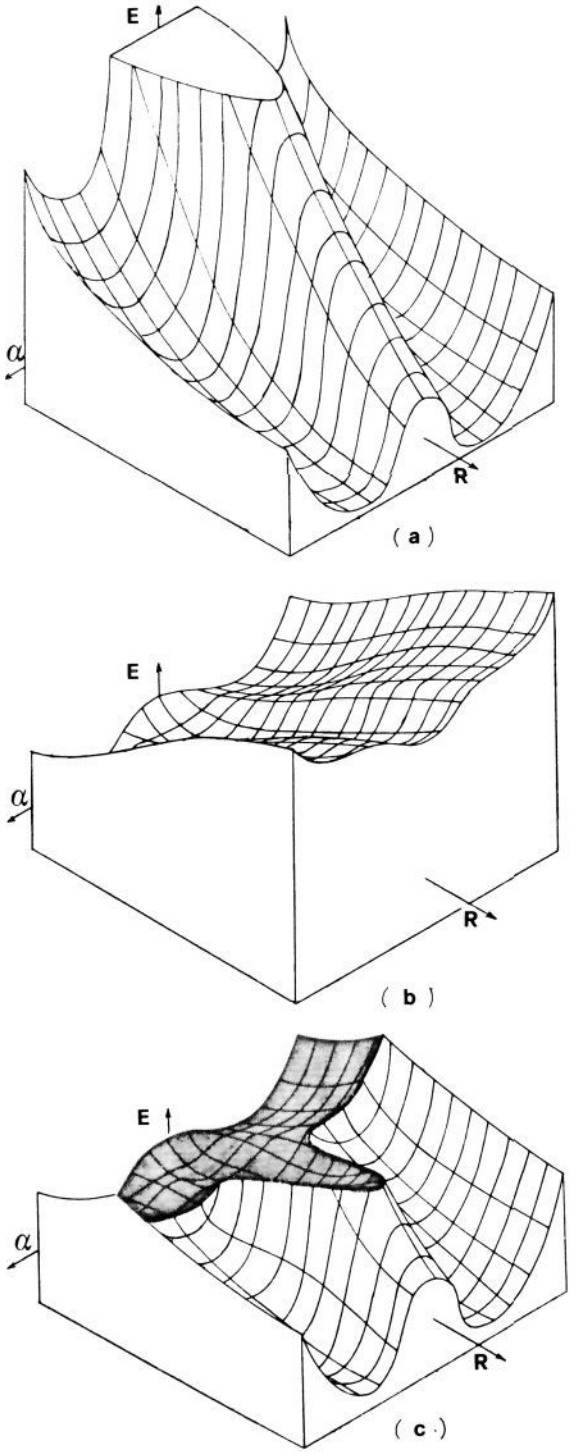

Figure 6. Diabatic surfaces in the R,α space: (a) reactant surface, (b) product surface, and (c) resulting surface.

increase with the decrease of R, the total energy of the reactant diabatic curve increases with the decrease of R. On the other hand, in the product interaction diagram, the dominant interactions are the stabilizing two-electron interactions π–π and π^*–π^*. Here, with the decrease of R, the overlap and related stabilization energy increase and the total energy of the product diabatic curve decreases.

It can also be observed (see Figure 5) that three of the critical points occur at similar R values, while the critical point associated with the D_{2h} rectangular supra–supra approach occurs earlier. In the latter case the destabilizing effect associated with the four-electron interaction π–π is larger and the related reactant diabatic

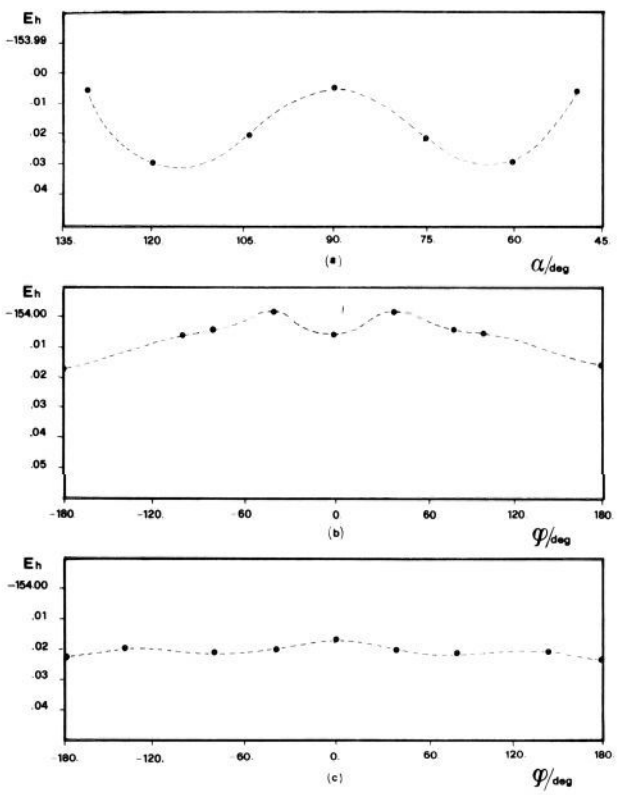

Figure 7. Curves of intersection in the R,α (a) and in the R,φ space [(b) with $\alpha = 90°$ and (c) with $\alpha = 117°$].

Scheme II

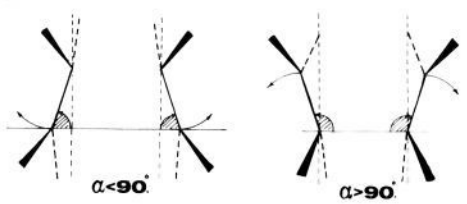

curve is more repulsive and consequently the crossing occurs earlier. In the former cases the effects are of similar order of magnitude and the crossings occur at similar R values.

The analysis so far has shown that for each type of approach there is an intersection of the two diabatic curves, corresponding to a critical point. However, with a two-dimensional analysis it is not possible to assess the real nature of the critical point. Therefore we have extended the analysis to include the other important internal coordinates and we have computed the corresponding three-dimensional surfaces. In the present case, in addition to R, the other important coordinates are α ($\alpha_1 = \alpha_2 = \alpha$) and φ (see Scheme I).

We examine first the diabatic surfaces associated with the supra–supra approach. According to the MC–SCF results, the supra–supra approach involves two second-order saddle points with index equal to 2. The lowest negative eigenvalue of the hessian matrix in each saddle point is clearly dominated by R, while the second negative eigenvalue is associated with α (in particular with the motions illustrated in Scheme II) in the case of the D_{2h} second-order saddle point and with φ in the case of the C_{2v} second-order saddle point.

To understand the origin of these different features we have computed the R,α and R,φ surfaces. The R,α surface is symmetric with respect to $\alpha = 90°$ (see Scheme II), while the R,φ surface is symmetric with respect to $\varphi = 0°$. In all cases the same geometrical parameters for the two ethylenic fragments have been used for each cross section along R. When appropriate, we have used the geometries of the critical points while, in the other cases,

interpolated geometries have been used, except for the R,φ surface at $\alpha = 90°$ where for the two ethylenic fragments we have used the geometrical parameters of the D_{2h} second-order saddle point for the whole surface.

Let us discuss first the two diabatic surfaces in the R,α space (see Figure 6); the corresponding curve of intersection is illustrated in Figure 7a. It can be seen that the shape of the two surfaces is completely different. The reactant diabatic surface increases rapidly with the decrease of R and shows a maximum for $\alpha = 90°$ at all values of R. On the other hand, the product diabatic surface decreases with the decrease of R and is almost flat with a slight minimum for $\alpha = 90°$ at all values of R. The features of the intersection of these two surfaces are illustrated in Figures 6c and 7a. The curve of intersection shows a maximum for $\alpha = 90°$ and a minimum for $\alpha = 117°$ (this is the value of α for the C_{2v} critical point). Therefore in the R,α space, the D_{2h} approach ($\alpha = 90°$) involves a saddle point with index equal to 2 and the C_{2v} approach ($\alpha = 117°$) a transition state corresponding to a minimum of the curve of intersection. The intersection for $\alpha = 90°$ occurs at $R = 2.3$ Å and the value of R at the intersection varies slightly with α and at $\alpha = 117°$ becomes $R = 1.92$ Å. It also can be observed that the shape of the curve of intersection is determined by the shape of the reactant surface.

These results can be rationalized in terms of simple MO arguments. The relevant MO interactions are shown in Figure 4. The reactant diabatic surface is associated with an interaction diagram where the two π MO's are doubly occupied and the dominant interaction is the four-electron destabilizing interaction π–π. When α becomes larger (or smaller) than 90°, the overlap between the two interacting MO's decreases and, according to eq 3, the destabilization decreases and then begins to increase again for larger (or smaller) values of α because of steric effects associated with the methylene group orbitals. On the other hand, the product diabatic surface is associated with an interaction diagram where the four MO's are singly occupied and the dominant interactions are the two stabilizing two-electron interactions π–π and π^*–π^*. The stabilization energy decreases with the increase of α, according to eq 5, since the overlap in both interactions decreases and consequently the total energy increases. The variation of the destabilization energy is much more pronounced than that of the stabilization energy, because in one case the energy effect is proportional to the square of the overlap while in the other just to the overlap.

Overlap integral values between the π and π^* MO's of the two interacting ethylenic fragments are listed in Tables I and II. These values have been computed at the STO-3G level in the framework of an SCF–MO computation. The behavior of the curve of intersection can be interpreted in terms of both types of interaction diagrams since along this curve the two diabatic surfaces have the same energy. However, the rationalization in terms of the interaction diagram associated with the dominant diabatic surface is more straitforward. In this case, when α becomes larger (or smaller) than 90°, there is a reduction of the destabilization and a lowering of the total energy, which eventually begins to increase because of steric effects.

The diabatic surfaces in the R,φ space are shown in Figure 8 for $\alpha = 90°$ and in Figure 9 for $\alpha = 117.7°$. The corresponding curves of intersection are illustrated in Figure 7, b and c. In both cases the reactant diabatic surface shows a maximum for $\varphi = 0°$ at all values of R and increases with the decrease of R, while the product diabatic surface shows a minimum at $\varphi = 0°$ and decreases with the decrease of R. These features are much more pronounced at $\alpha = 90°$ than at $\alpha = 117°$. The shape of the curve of intersection is dominated by the product surface for $\alpha = 90°$ and by the reactant surface for $\alpha = 117°$: consequently this curve shows a minimum for $\alpha = 90°$ and a maximum for $\alpha = 117°$.

These different forms of behavior again can be rationalized in terms of simple MO arguments. The shape of the reactant surface is determined by the energy variation of the four-electron destabilizing interaction. The π–π overlap and related destabilization decrease with the increase of the absolute value of φ and increase with the decrease of R (see Table I). On the other hand, the shape

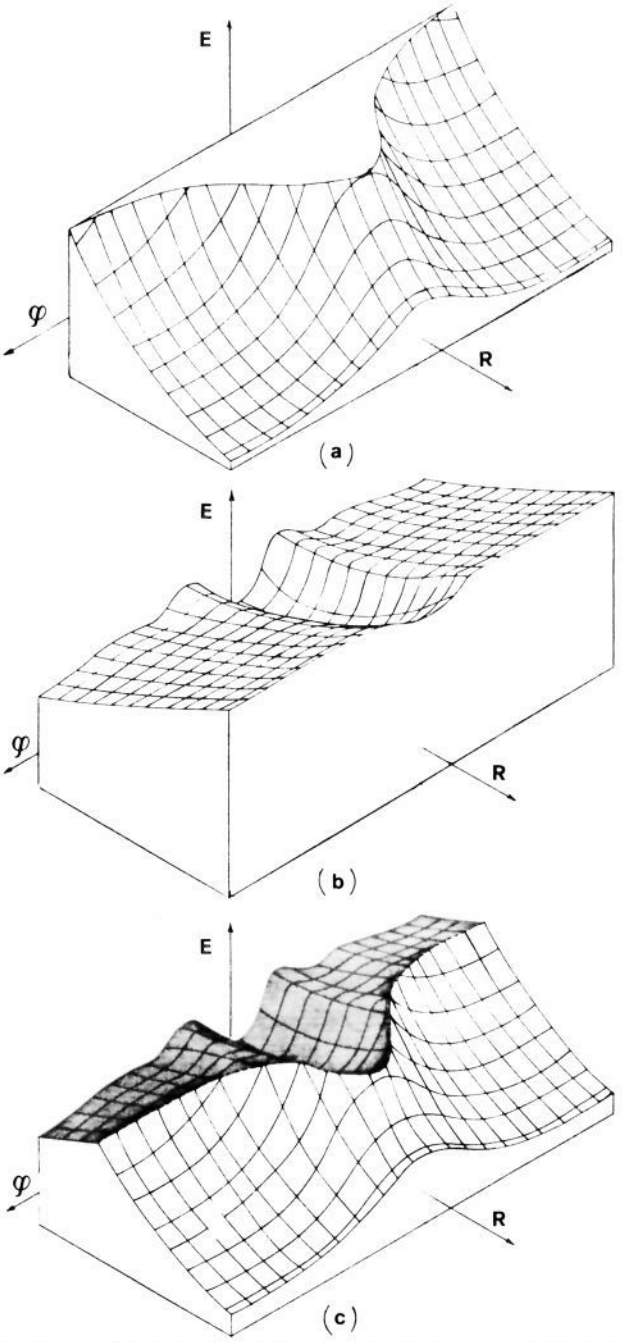

Figure 8. Diabatic surfaces in the R,φ space ($\alpha = 90°$): (a) reactant surface, (b) product surface, and (c) resulting surface.

of the product surface is determined by the energy variation associated with the stabilizing two-electron interactions. The π–π, π^*–π^* overlaps and the related stabilizations decrease with the increase of the absolute value of φ and increase with the decrease of R (see Table I). At $\alpha = 90°$ the rate of change of the overlaps with φ is slightly slower than that occurring with α at $\varphi = 0°$. This has the effect of making the reactant surface less repulsive, while the product surface is only slightly affected. In this situation the crossing is dominated by the product surface. At $\alpha = 117°$, the rate of change of the overlaps with φ is even smaller. In this case the product surface is almost flat and the crossing is dominated by the reactant surface.

It can be seen that the curve of intersection at $\alpha = 117°$ shows a maximum at $\varphi = 0°$ and in the range 0–180° two minima (at $\varphi \simeq 60°$ and 180°, respectively) and another maximum at $\varphi \simeq 120°$. As previously pointed out, the minima on this curve correspond to transition states in the subspace under examination.

Table I. Values of the Overlap Integrals between the π and π^* MO's of the Two Interacting Ethylenic Fragments at Various Values of φ

	R = 2.2263 Å, α = 90°			R = 1.9192 Å, α = 117.72°		
φ, deg	$\pi-\pi$	$\pi-\pi^*$	$\pi^*-\pi^*$	$\pi-\pi$	$\pi-\pi^*$	$\pi^*-\pi^*$
0	0.1986	0.0000	0.1693	0.1913	0.1335	0.1180
30	0.1792	0.0000	0.1342	0.1894	0.1351	0.1156
60	0.1399	0.0000	0.0797	0.1850	0.1377	0.1126
90	0.1283	0.0000	0.0573	0.1800	0.1390	0.1131
120	0.1264	0.0000	0.0496	0.1757	0.1393	0.1147
150	0.1277	0.0000	0.0445	0.1732	0.1394	0.1146
180	0.1285	0.0000	0.0421	0.1725	0.1394	0.1140

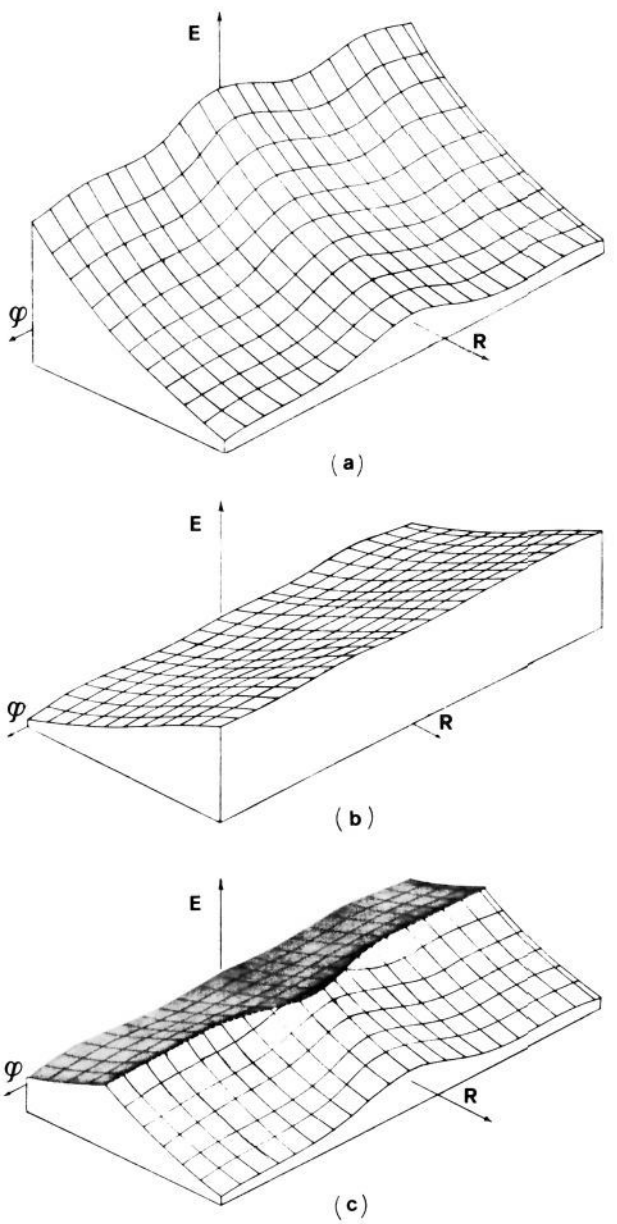

Figure 9. Diabatic surfaces in the R,φ space (α = 117°): (a) reactant surface, (b) product surface, and (c) resulting surface.

Since for large values of φ changes in α have a negligible effect, these two minima are real transition states for the whole space and correspond to the gauche and trans fragmentation transition states.

The other critical points of this surface, i.e., the gauche and trans minima and the transition states connecting the two minima and the gauche minimum to cyclobutane, all lie on the part of the adiabatic surface dominated by the product diabatic surface.

Table II. Values of the Overlap Integrals between the π and π^* MO's of the Two Interacting Ethylenic Fragments at Various Values of α (R = 2.2263 Å, φ = 0°)

α, deg	$\pi-\pi$	$\pi-\pi^*$	$\pi^*-\pi^*$
90	0.1986	0.0000	0.1693
100	0.1398	0.0552	0.1117
110	0.1102	0.0784	0.0890
120	0.0914	0.0806	0.0805
130	0.0765	0.0735	0.0738

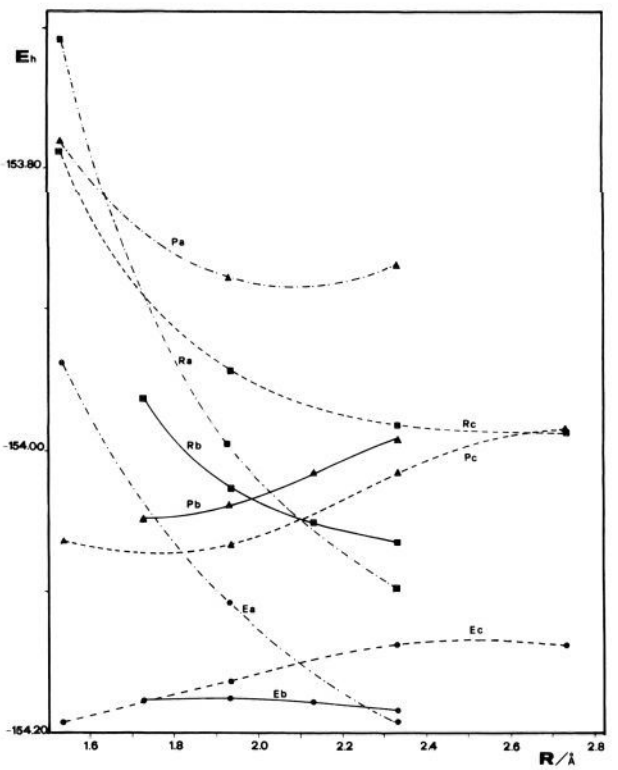

Figure 10. Reactant (R) and product (P) diabatic and related adiabatic curves for a trans approach computed with different C–C bond lengths appropriate for (a) the reactants (r_{cc} = 1.306 Å), (b) the products (r_{cc} = 1.507 Å), and (c) the critical point (r_{cc} = 1.419 Å).

Therefore, while the gauche and trans fragmentation transition states originate from the crossing of the two diabatic surfaces, the gauche–trans and the *gauche*-cyclobutane transition states originate from conformational effects.

The previous diabatic surfaces have been computed by using for the two ethylenic fragments the geometrical parameters of the various critical points. To obtain information about the effect of geometrical changes upon the diabatic curves, we have performed computations using for the ethylenic fragments C–C bond lengths appropriate for the reactants (r_{c-c} = 1.306 Å), for the products (r_{c-c} = 1.507 Å), and for the critical point (r_{c-c} = 1.419 Å). The related diabatic and adiabatic curves are shown in Figure 10 for the trans approach. The behavior of these curves for the other types of approach is very similar.

Here, in all cases, there is an intersection of the related diabatic curves. With the increase of the ethylenic C–C bond length, the intersection occurs earlier, because the reactant asymptote is raised and the product one is lowered. As a consequence for distances between the two fragments greater than 2.5 Å where the reactant diabatic curve is dominant, the adiabatic curve with the lowest energy is that associated with the ground-state ethylene geometry, while at shorter distance where the product diabatic curve is dominant the adiabatic curve with the lowest energy becomes that associated with the stretched ethylenic C–C bond. Here the intersection of the adiabatic curves is not real, since they represent different cross sections of the whole surface.

IV. Conclusion

In this paper we have analyzed the cycloaddition of two ethylene molecules in terms of diabatic surfaces. We have shown that this analysis provides a clear understanding of the index and origin of the various critical points. We have also shown that the behavior of the constituent diabatic surfaces as well as that of the curve of intersection can be easily rationalized by using simple MO energy expressions.

Registry No. Ethylene, 74-85-1.

Aromaticity of Highly Bent Benzene Rings. An Investigation by High Field Deuterium NMR of [5]Metacyclophane and Model Compounds

P. C. M. van Zijl, L. W. Jenneskens, E. W. Bastiaan, C. MacLean,* W. H. de Wolf, and F. Bickelhaupt*

Contribution from the Chemical Laboratory, Free University, De Boelelaan 1083, 1081 HV Amsterdam, The Netherlands. *Received September 19, 1985*

Abstract: High field deuterium NMR provides a new and simple method for establishing the degree of aromaticity of a compound. The procedure is based on the determination of the magnetic susceptibility anisotropy from quadrupolar deuterium couplings of molecules in solution aligned by the magnetic field. The technique is illustrated for some deuterated dialkylbenzenes (**2d**, **3e**, **4e**) and applied to [8,11-$^2H_2$][5]metacyclophane (**1d**). Surprisingly, **1d** is found to be fully aromatic in spite of its strongly bent benzene ring.

One of the most discussed topics in chemistry is undoubtedly the concept of aromaticity.[1-4] Although no general definition of aromaticity is available, a commonly accepted description is in terms of π-electron delocalization in a ring, which causes resonance stabilization.[5] Widely used criteria for aromaticity are the following:[1] the structure of the rings (planarity, bond lengths), heat of formation of the compound, reactivity of ring subtituents, and the presence of "ring-currents". The existence of ring-currents is a subject of discussion;[6] a better criterion is the magnetic susceptibility χ, which is directly related to the electronic structure of a molecule. Dauben et al.[7] suggested that the magnetic susceptibility exaltation, defined by

$$\Omega = \chi(\text{obsd}) - \chi(\text{local}) \quad (1)$$

is a measure for aromaticity. Here $\chi = 1/3(\chi_{xx} + \chi_{yy} + \chi_{zz})$ is the average molecular susceptibility, with x, y, z the principal axes of the susceptibility tensor. χ(local) is χ of a nonaromatic reference molecule calculated by means of known localized susceptibilities. Recently, Aihara[4] demonstrated that Ω is related to the resonance energy of the ring. An analogous measure of aromaticity is the enhancement Δ of the absolute value of the susceptibility component perpendicular to the ring, χ_{zz}, or, since the in-plane components of aromatic molecules and their nonaromatic analogues are about the same,[8] the change in the magnetic susceptibility anisotropy $\Delta\chi$

$$\Delta = \chi_{zz}(\text{obsd}) - \chi_{zz}(\text{local}) \approx \Delta\chi(\text{obsd}) - \Delta\chi(\text{local}) \quad (2)$$

Flygare et al.[8-10] demonstrated the applicability of this procedure for a series of aromatic and nonaromatic molecules. The method has been criticized by Benassi et al.[11] on the ground of semiempirical calculations. However, their criticism is dubious, since it only applies to Δ-values which are of the order of magnitude of the experimental error of the used local susceptibility values. In other cases the approach will be able to give a quantification of the aromatic character of the compound.

Compounds for which the question of aromaticity is of particular interest are the short-bridged cyclophanes,[12] where the benzene ring aromaticity may be influenced by the bending imposed by the bridge. In the [n]metacyclophane series, [5]metacyclophane (**1a**) is the shortest known representative. Indeed, large deviations from planarity of the benzene ring were revealed in the X-ray crystal structure of a derivative of **1a**: 8,11-dichloro-[5]metacyclophane (**1b**); the molecule possesses C_s symmetry and the benzene ring has an asymmetrical boat conformation, with the bow bending about 27° and the stern 12° out of the plane of the ring.[13] This geometry is reasonably well reproduced by MNDO[14,15] and MM[16] calculations. A surprising feature of the crystal structure is the length of the bonds in the benzene ring. Whereas the possibility of bond fixation toward a cyclohexatriene-like structure had been discussed in view of the strongly enhanced chemical reactivity of **1a** and **1b**,[17] the actually observed bond lengths (1.393 ± 0.007 Å) are uniform within experimental error and typical for a delocalized aromatic molecule. Furthermore, the chemical shifts of the benzene ring protons of **1a–c** are in the low-field region (about 6.5–8 ppm)[15,18] and it seems plausible

(1) Lewis, D.; Peters, D. *Facts and Theories of Aromaticity*; Macmillan: New York, **1975**; also references therein.
(2) Balaban, A. T. *Pure Appl. Chem.* **1980**, *52*, 1409.
(3) Mallion, K. B. *Pure Appl. Chem.* **1980**, *52*, 1541.
(4) Aihara, J. *J. Am. Chem. Soc.* **1979**, *101*, 558; **1981**, *103*, 5704.
(5) Hückel, E. *Z. Phys.* **1931**, *70*, 204; **1931**, *72*, 310. Hückel, E. *Grundzüge der Theorie Ungesättigter und Aromatischer Verbindungen*; Verlag Chemie: Berlin, 1938; p 71.
(6) Musher, J. I. *J. Chem. Phys.* **1967**, *46*, 1219.
(7) Dauben, H. J., Jr.; Wilson, J. D.; Laity, J. L. *J. Am. Chem. Soc.* **1968**, *90*, 811; **1969**, *91*, 1991.
(8) Sutter, D. H.; Flygare, W. H. *Topics in Current Chemistry*; Springer: Berlin, 1976; Vol. 63, p 89.
(9) Benson, R. C.; Flygare, W. H. *J. Chem. Phys.* **1973**, *58*, 2366.
(10) Schmalz, T. G.; Norris, C. L.; Flygare, W. H. *J. Chem. Phys.* **1973**, *95*, 7961.
(11) Benassi, R.; Lazzeretti, P.; Taddei, F. *J. Phys. Chem.* **1975**, *79*, 848.
(12) For a review: *Cyclophanes*; Keehn, P. M., Rosenfeld, S. M., Eds.; Academic: New York, 1983.
(13) Jenneskens, L. W.; Klamer, J. C.; De Boer, H. J. R.; De Wolf, W. H.; Bickelhaupt, F.; Stam, C. H. *Angew. Chem.* **1984**, *96*, 236.
(14) Turkenburg, L. A. M.; De Wolf, W. H.; Bickelhaupt, F.; Cofino, W. P.; Lammertsma, K. *Tetrahedron Lett.* **1983**, *24*, 1821.
(15) Jenneskens, L. W.; De Kanter, F. J. J.; Turkenburg, L. A. M.; De Boer, H. J. R.; De Wolf, W. H.; Bickelhaupt, F. *Tetrahedron* **1984**, *40*, 4401.
(16) Carballeira, L.; Pereiras, A. J.; Rios, M. A. *J. Chem. Phys.* **1984**, *80*, 4387.
(17) Turkenburg, L. A. M.; Blok, P. M. L.; De Wolf, W. H.; Bickelhaupt, F. *Angew. Chem.* **1982**, *94*, 291.

0002-7863/86/1508-1415$01.50/0